

**UCC Library and UCC researchers have made this item openly available.
 Please [let us know](#) how this has helped you. Thanks!**

Title	Nitrogen-doped carbon nanotubes: growth, mechanism and structure
Author(s)	O'Byrne, Justin P.; Li, Zhonglai; Jones, Sarah L. T.; Fleming, Peter G.; Larsson, J. Andreas; Morris, Michael A.; Holmes, Justin D.
Publication date	2011-10-14
Original citation	O'Byrne, J. P., Li, Z., Jones, S. L. T., Fleming, P. G., Larsson, J. A., Morris, M. A. and Holmes, J. D. (2011) 'Nitrogen-Doped Carbon Nanotubes: Growth, Mechanism and Structure', ChemPhysChem, 12(16), pp. 2995-3001. doi: 10.1002/cphc.201100454
Type of publication	Article (peer-reviewed)
Link to publisher's version	https://onlinelibrary.wiley.com/doi/abs/10.1002/cphc.201100454 http://dx.doi.org/10.1002/cphc.201100454 Access to the full text of the published version may require a subscription.
Rights	© 2011 Wiley-VCH Verlag GmbH & Co. KGaA, Weinheim. This is the peer reviewed version of the following article: (2011), Nitrogen-Doped Carbon Nanotubes: Growth, Mechanism and Structure. ChemPhysChem, 12: 2995-3001, which has been published in final form at https://doi.org/10.1002/cphc.201100454 . This article may be used for non-commercial purposes in accordance with Wiley Terms and Conditions for Self-Archiving.
Item downloaded from	http://hdl.handle.net/10468/6696

Downloaded on 2021-11-27T05:59:28Z

DOI: 10.1002/cphc.200((will be filled in by the editorial staff))

Nitrogen-Doped Carbon Nanotubes: Growth, Mechanism and Structure

Justin P. O'Byrne^{[a], [b]}, Zhonglai Li^{[a], [b]}, Sarah L. T. Jones^[c], Peter G. Fleming^{[a], [b]}, J. Andreas Larsson^[c], Michael A. Morris^{[a], [b]} and Justin D. Holmes^{[a], [b],*}

Nitrogen-doped bamboo-structured carbon nanotubes have been successfully grown using a series of cobalt/molybdenum catalysts. The morphology and structure of the nanotubes were analysed by transmission electron microscopy and Raman spectroscopy. The level of nitrogen doping, as determined by X-ray photoelectron spectroscopy, was found range between of 0.5 to 2.5 at. %. The

growth of bamboo-structured nanotubes in the presence of nitrogen, in preference to single-walled and multi-walled nanotubes, was due to the greater binding energy of nitrogen for cobalt in the catalyst compared to the binding strength of carbon to cobalt, as determined by density functional theory.

Introduction

The extraordinary electronic properties of carbon nanotubes (CNTs) makes them a potential material for many nanoelectronic applications, including transistor channels and interconnects^[1]. However, for such applications control over the structure and electronic properties of nanotubes will have to be achieved, potentially requiring doping of their structures^[2]. Nitrogen is an obvious dopant candidate for CNTs, as the size of nitrogen relative to carbon is quite similar and as such should not cause excessive disruption to the nanotube lattice^[3]. The incorporation of nitrogen into a graphitic lattice can take place in one of two ways; as graphene-like or pyridine-like nitrogen^[4]. In graphene-like incorporation, nitrogen binds in the same way as carbon, *i.e.* with 3 bonds to other carbons. In the case of pyridine-like inclusion, the nitrogen is bound to 2 carbon atoms^[5]. Previous reports of bamboo-structured carbon nanotubes (BCNTs) indicate that nitrogen doping levels can range from <1 to 20 at. %^[6]. Nitrogen-doped carbon nanotubes have consistently been reported as being bamboo-structured^[6-7]. Other dopant atoms that have been incorporated into carbon nanotubes include boron and phosphorus^[8]. Larger atoms including cesium and potassium have also been introduced between bundles of nanotubes^[4b].

The growth of single walled carbon nanotubes (SWNTs), multi-walled carbon nanotubes (MWNTs) and BCNTs follow similar pathways^[9]. Typically, a catalyst particle cracks the feedstock gas and supports the resultant intermediate carbon species formed on its surface. The catalyst particle provides a surface template for carbon-carbon bond formation resulting in cap-shaped graphitic flakes, *i.e.* nanotube nucleation^[9]. SWNT and MWNT growth follow very similar mechanisms where the carbon source is continuously cracked and uninterrupted tube growth begins; stopped only by discontinuation of the supply of carbon feedstock, catalyst poisoning or encapsulation of the catalyst by graphitic carbon^[10]. The nucleation of a nanotube on

a metal nanoparticle surface is intrinsically linked with metal-carbon binding strengths, growth temperature and nanoparticle size. If it is energetically favourable for carbons on the surface to bind to one another, dome-shaped graphitic flakes will form. In the case of BCNTs, the process of forming dome shaped graphitic flakes continuously repeats, leading to characteristic chamber formation. The stabilisation of carbon atoms on the surface of a nanoparticle catalyst increases as its diameter decreases, due to the increasing surface energy of the nanoparticles^[11]. In fact, the binding energy of a nanoparticle to carbon plays a vital role in the growth of CNTs, as this energy must obey a "Goldilocks" criterion. If the binding energy of the nanoparticle to carbon is too low, the nanoparticle will not support the growing end of a nanotube and no tube formation occurs. On the other hand, if the binding energy is too high, a carbide will preferentially form on the surface of the nanoparticle, which leads to poisoning of the catalyst. The catalyst binding energy to carbon must therefore be within a certain window to promote nanotube growth^[12]. BCNT growth is slightly different compared to MWNT growth in that the graphitic layers formed bind more strongly to the catalyst nanoparticle, sometimes caused by stronger bonds to one of the metals in an alloy catalyst^[12c, 12d]. As the reaction progresses, the catalyst cracks more carbon and causes inner layers of CNTs to grow; strong metal-graphene

[a] Dr Justin P. O'Byrne, Dr Zhonglai Li, Dr Peter G. Fleming, Prof Michael A. Morris, Justin D. Holmes*
Materials & Supercritical Fluids Group
Department of Chemistry & the Tyndall National Institute
University College Cork, Cork, Ireland
Fax: (+353) 21 4274097
E-mail: j.jolmes@ucc.ie

[b] Dr Justin P. O'Byrne, Dr Zhonglai Li, Dr Peter G. Fleming, Prof Michael A. Morris, Justin D. Holmes*
Centre for Research on Adaptive Nanostructures and Nanodevices (CRANN)
Trinity College Dublin, Dublin 2, Ireland

[c] Ms Sarah L. T. Jones, Dr J. Andreas Larsson
Electronics Theory Group
Tyndall National Institute, Cork, Ireland

binding causes local “pin points”, leading to repeated elongation of the nanoparticle and characteristic chamber formation. When the surface energy of the nanoparticle increases beyond the stabilisation energy afforded by being bound to the CNT inner shell, the nanoparticle retracts to its lowest surface energy shape (spherical) and the process repeats^[13]. Defects are to be expected when BCNTs are formed because of the increased amount of edges present. In this article we show that deformation of the catalyst nanoparticle, due to prolonged bonding at local “pin points” caused by nitrogen-metal interactions, is the driving force behind BCNT growth.

Results and Discussion

Carbon Nanotube Growth and Nitrogen Doping

Various Co/Mo catalysts were used for the growth of nitrogen-doped (N-doped) carbon nanotubes. 4 wt. % Co/3 wt. % Mo catalysts supported on MgO were used to grow SWNTs by the chemical vapour deposition (CVD) of methane at 850 °C (see Figure 1(a)). Upon the addition of a nitrogen source to the gas mixture, in the form of ammonia, acetonitrile or pyridine, BCNTs formed in preference to either SWNTs or MWNTs. Consequently, adding a nitrogen source to the feedstock gas for a catalyst that under normal conditions produces SWNTs, causes the formation of BCNTs. Figures 1(b), (c) and (d) shows transmission electron microscopy (TEM) images of the carbon products formed when nitrogen sources of ammonia, acetonitrile and pyridine were added respectively to the feed-stock gas during the CVD process. The general morphologies of the nanotubes formed were the same for all of the nitrogen sources investigated.

Figures 2(b), (c) and (d) show Raman spectra obtained from N-doped BCNTs generated using methane with acetonitrile, pyridine and ammonia respectively as the nitrogen sources. The graphitisation, the relationship between the G-band intensity (I_G) against the D-band intensity (I_D), was used to determine the crystallinity of the samples^[14]. The I_D/I_G ratio of the purified SWNTs synthesised from a 4 wt. % Co/3 wt. % Mo catalyst, supported on MgO in the absence of nitrogen, was found to be 0.11, as shown in figure 2(a). Previous reports on BCNT growth have shown the I_D/I_G ratio to be approximately equal^[15]. The I_D/I_G ratio of the BCNTs grown using acetonitrile and pyridine as nitrogen sources were found to be 1.14 and 1.16 respectively, as shown in figures 2 (b), (c) and (d), indicating that the nanotubes produced in this study were reasonably well graphitised but also contained a number of structural defects. The I_D/I_G ratio of nanotubes grown using ammonia as a nitrogen source was found to be a mean value of 0.53, suggesting that these nanotubes were better graphitised and contained fewer defects than those grown from acetonitrile and pyridine. The difference in the graphitisation of the N-doped nanotubes generated can be attributed to the surplus of carbon atoms in acetonitrile and pyridine compared to ammonia, resulting in disruption of the structure and graphitisation of the nanotubes generated. The nitrogen content of BCNTs formed varied from 1 to 2.5 % for all nitrogen sources investigated. The nitrogen content may be related to the binding strength of the catalyst to nitrogen. For Co/Mo catalysts, the binding energy of carbon to the catalytic metals is within a window for growth where carbon-carbon bond formation favourably replaces carbon-metal bonds and tube growth occurs. As nitrogen-cobalt bonding is stronger than carbon-cobalt bonding, replacing a nitrogen-cobalt bond with a

nitrogen-carbon bond during tube growth is unfavourable. Table 1 shows the nitrogen content of nanotubes grown from various Co/Mo catalyst, as determined by X-ray photoelectron spectroscopy (XPS). From either method of introducing nitrogen, flowing Ar over a nitrogen source or using gaseous ammonia, the nitrogen content did not exceed ~2.5 atom %. BCNTs that were N-doped through the inclusion of NH_3 as a feedstock gas had one of the highest doping levels and level of graphitisation of all of the samples produced.

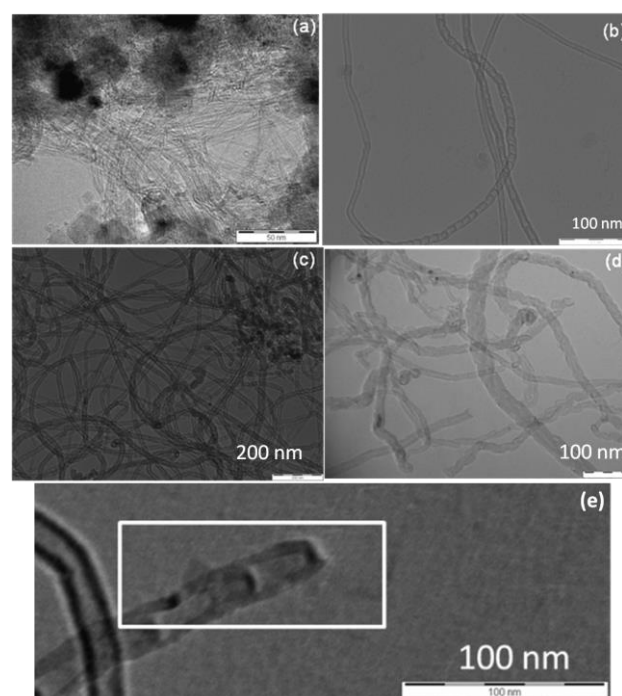


Figure 1. TEM images of nanotubes synthesised from a 4 wt. % Co/3 wt. % Mo catalyst supported on MgO; (a) SWNTs generated in the absence of nitrogen, (b) nanotubes synthesised in the presence of ammonia, (c) nanotubes synthesised from acetonitrile as the nitrogen source, (d) BCNTs grown using pyridine as a nitrogen source, (e) tip of tube showing the thickness of the nanotube tip being the same as the chamber tip.

Theoretical Calculations

From previous calculations, the binding energy of metal nanoparticles to the end of a nanotube falls within a nanotube growth window which varies from tube to tube^[12a-c]. The binding strength of a nanoparticle to carbon is extremely important, if the binding strength is too low, the growing nanotube end is not sufficiently stabilised and growth will not occur. If the carbon-metal binding strength is too high, carbon-carbon bond formation is unfavourable and a metal carbide will result. The effect of nitrogen incorporation on the binding strengths of CNTs bound to Co nanoparticles were modelled using four systems: Co_{13} bonded to a (3,3) and a (5,0) tube; and Co_{55} bonded to a (5,5) and a (10,0) tube (see figure 3), by placing nitrogen in Layer 1-4, computing the dissociation energy and comparing to the

corresponding undoped tubes (see table 2). In the majority of Layer 2-4 cases a larger binding energy to the metal than for carbon per bond was observed, $\Delta E/\text{bond}$, which means that the nitrogen dopant strengthens the interaction between the growing nanotube and the metal catalyst particle.

However, in the Layer 1 cases the $\Delta E/\text{bond}$ values are consistently smaller than for the equivalent undoped cases, which would mean that the incorporation of nitrogen into the CNTs weakens the interaction between the nanotube and the catalytic metal particle when nitrogen is directly bonded to the metal. However this is likely an artefact arising from using dissociation energies as a measure of bond strengths, since the calculation is made using the energy difference between a bound nanoparticle and nanotube and an unbound fragmented state. The difference in fragment stabilisation of the dissociated products are reflected in the $\Delta E/\text{bond}$ values^[16]. The incorporation of nitrogen strengthens the CNT-metal interaction, as seen by comparing the total energies in table 2: The total energies of the Layer 1 complexes are consistently lower than the corresponding Layer 2-4 total energies, as exemplified by the Co_{55} -(5,5) complex in figure 4 (complex energy stabilisation). The Layer 1 complex energy is 0.624 eV lower than in the Layer 2 complex for the Co_{13} -(3,3) case, 1.019 eV lower for Co_{55} -(5,5), 0.328 eV lower for Co_{13} -(5,0), and 0.714 eV lower for the Co_{55} -(10,0) case.

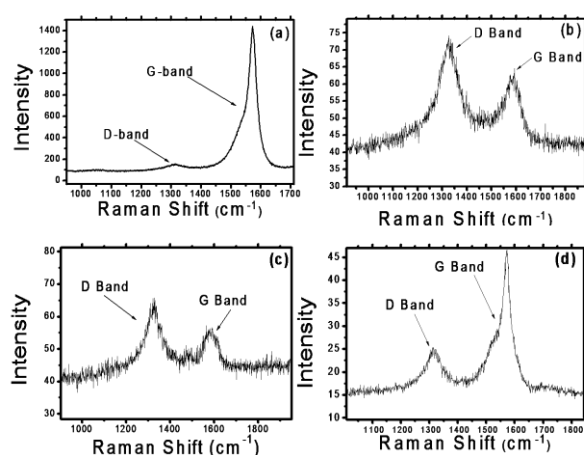


Figure 2. Raman spectrum of nanotubes synthesised from the CVD of methane over a 4 wt. % Co/3 wt. % Mo supported on a MgO support: (a) purified SWNTs, (b) purified N-doped BCNTs using acetonitrile, (c) purified N-doped BCNTs grown using pyridine as nitrogen source and (d) BCNTs doped with nitrogen using ammonia.

Table 1. Table showing the nitrogen content of BCNTs generated by the CVD of various carbon and nitrogen sources over Co/Mo catalysts

Catalyst (on MgO)	C-source	N-source	Temp. (°C)	Wt.% C	Wt.% N
4% Co/12% Mo	CH ₄	C ₅ H ₅ N	750	99.5	0.5
4% Co/6% Mo	CH ₄	C ₅ H ₅ N	750	99.4	0.6
3% Co/4% Mo	CH ₄	C ₅ H ₅ N	800	98.9	1.1
3% Co/4% Mo	CH ₄	C ₅ H ₅ N	700	98.2	1.8
3% Co/2% Mo	CH ₄	CH ₃ CN	850	98.1	1.9
3% Co/2% Mo	CH ₃ CN	CH ₃ CN	850	98.4	1.6
3% Co/2% Mo	CH ₄	NH ₃	850	98.1	1.9
4% Co/3% Mo	CH ₄	CH ₃ CN	850	98.2	1.8
4% Co/3% Mo	CH ₄	NH ₃	850	97.5	2.5
4% Co/3% Mo	CH ₄	C ₅ H ₅ N	850	98.4	1.6

In the $\Delta E/\text{bond}$ binding energies the stronger binding in the Layer 1 complexes is counteracted by very large fragment

stabilisation of the Layer 1 dissociated tubes (see figure 4, product energy stabilisation), where the nitrogen atom has two binding partners instead of three as when nitrogen is in Layers 2 to 4. Comparing the Layer 2 dissociated tubes, the Layer 1 total energies is 1.970 eV lower in the (3,3) case, 1.871 eV lower for the (5,5) case, 1.462 eV lower for (5,0), and 1.694 eV lower for the (10,0) case (see table 1). These fragment stabilisation energies for the dissociated tubes are much larger than the decrease in the complex total energies in the Layer 1 cases compared to Layer 2, as illustrated in the case of Co_{55} -(5,5) in figure 4. The “product energy stabilisation” is always larger than the “complex energy stabilisation” for nitrogen in Layer 1 compared to Layer 2. The nitrogen atom present in Layer 1 causes a very stable situation with nitrogen on the tube edge with only two neighbours. A nitrogen atom in this place artificially results in decreased dissociation energies, and $\Delta E/\text{bond}$ values, for the Layer 1 cases, although the CNT-metal interaction is in fact strongest in the Layer 1 cases.

Table 2. Total energies for all cobalt particle/CNT complexes and the corresponding unbound tube fragments with nitrogen replacing one carbon atom in Layer 1 – 4 (see figure 3), and tube – metal binding energies ΔE . The total energy for the Co_{13} cluster is -66.896 eV, and -329.091 eV for the Co_{55} cluster.

	Co_{13} -(3,3)			Co_{13} -(5,0)		
	E_{tube} (eV)	E_{complex} (eV)	$\Delta E/\text{bond}$ (eV)	E_{tube} (eV)	E_{complex} (eV)	$\Delta E/\text{bond}$ (eV)
Layer 1	-326.552	-403.864	-1.736	-264.462	-345.567	-2.842
Layer 2	-324.583	-403.240	-1.960	-263.000	-345.239	-3.069
Layer 3	-324.616	-402.991	-1.913	-262.869	-345.186	-3.084
Layer 4	-324.663	-403.050	-1.915	-262.691	-345.350	-3.153
Undoped	-326.320	-404.189	-1.865	-264.226	-346.208	-3.018
	Co_{55} -(5,5)			Co_{55} -(10,0)		
	E_{tube} (eV)	E_{complex} (eV)	$\Delta E/\text{bond}$ (eV)	E_{tube} (eV)	E_{complex} (eV)	$\Delta E/\text{bond}$ (eV)
Layer 1	-558.693	-904.443	-1.666	-548.608	-905.132	-2.743
Layer 2	-556.822	-903.424	-1.751	-546.914	-904.418	-2.841
Layer 3	-556.777	-903.566	-1.770	-545.469	-904.065	-2.951
Layer 4	-556.726	-903.351	-1.753	-546.366	-904.197	-2.874
Undoped	-558.388	-905.065	-1.759	-549.525	-905.347	-2.673

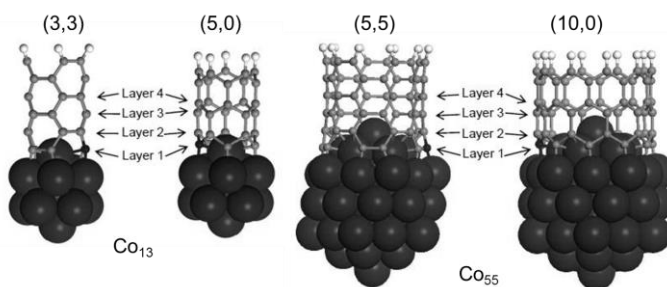


Figure 3. Schematic of the (3,3) and (5,0) nanotube bound to a Co_{13} metal cluster, and the (5,5) and (10,0) nanotubes bound to a Co_{55} metal cluster, with a nitrogen atom replacing a carbon atom in Layer 1, Layer 2, Layer 3 and Layer 4. The Co atoms are coloured dark, C light grey, H white, and N black.

Similar increases in tube-metal binding energies have been reported to explain why the non-conventional nanocomposite Cu/Mo^[12c], Cu/W and Pd/Mo^[12d] can be used as catalysts for CNT growth, which result in similar BCNT growth due to local pin-pointing by the strong binding metal atoms (either Mo or W) on

the surface of nanocomposite particles. In the present study the stronger bonds leading to pin-pointing is due to nitrogen incorporation into the CNT graphitic structure, but the resulting growth mechanism is the same, leading to a BCNT product.

Analysis of the Growth Mechanism

In the formation of SWNTs and MWNTs, the graphitic carbon structure interacts with the nanoparticle, increasing the stability of the surface atoms on the nanoparticle. This stabilisation causes the nanoparticle to elongate during the second stage of growth as more carbon is supplied to the cap edge. As the nanoparticle elongation increases, the energy needed to stabilise it increases to a point where being bound to the graphitic layer is no longer favourable. The carbon layer bound to the surface cannot energetically compete with the metal contraction as the metal is losing metal-metal bonds in favour of more and more surface atoms. When the stabilisation of the surface atoms of the metal by the inner most carbon layer becomes less than the surface energy afforded by being in a more stable shape, the nanoparticle contracts back to a more stable spherical shape. Upon this contraction growth continues into its third phase, with the carbons from the nanoparticle adding to the growing edge of the nanotube. However, for BCNTs, the process of elongation during cap formation repeats and further elongations and contractions of the metal particle happen through new carbon capping of the particle surface^[13]. We have observed the formation of BCNTs when incorporating nitrogen into the nanotube structure, although using the same growth conditions in the absence of nitrogen results in the formation of SWNTs. Our simulations show that nitrogen itself acts as a local pin-pointing agent between the forming CNT and the catalyst particle and thus explains the observed BCNT product (see discussion below).

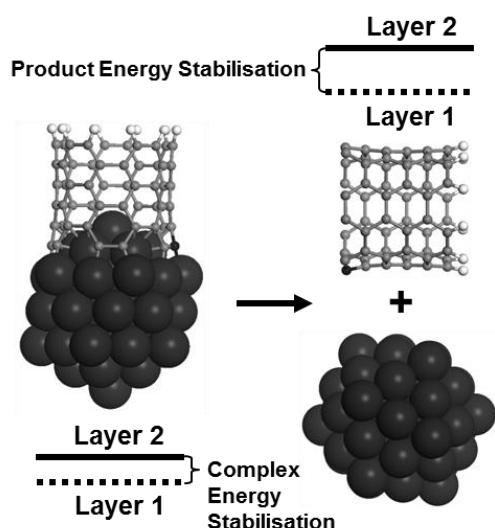


Figure 4. Energy levels showing the increased stabilisation of nitrogen in Layer 1 compared to Layer 2 for the Co₅₅-(5,5) complex (left hand side), and the much larger stabilisation of the dissociated products with nitrogen in Layer 1 compared to Layer 2 (right hand side) that is entirely due to the difference in the N-doped tube fragment. These two effects result in a smaller dissociation energy for Layer 1 than for Layer 2, although the tube is bonded more strongly when nitrogen is in Layer 1. The Co atoms are coloured dark grey, C light grey, H white, and N black.

From HRTEM images shown in figure 5, the thickness of the carbon layers was observed to differ throughout the nanotube chamber. At the “tip” of the chamber the number of carbon layers was significantly higher than at the “base” and sidewalls of the chamber. The TEM image of the BCNTs shows the chamber tip with 12 graphitic layers, while the side walls by the tip have approximately 20 layers. This is in contrast to the base walls of the chamber which typically have about 7 layers. The difference in the wall thickness of the BCNT from the tip to the bottom chamber can be attributed to the mechanism by which the BCNTs form. In-situ TEM measurements taken by Helveg *et al.*^[13] and Lin *et al.*^[17], showed that the number of layers in the nanotube structure grows as the nanoparticle residency time increases. The bamboo structure of the nanotube can be regarded as a “fingerprint” of the growth mechanism, where the thickness of the sidewalls provides information on the length of time the catalyst particle is resident in a particular location, measured here by the wall thickness. The bamboo structure forms preferentially over more crystalline MWNTs during nitrogen doping due to a greater binding strength difference between the nanoparticle and a nitrogen-doped graphitic structure compared to the undoped case; the nitrogen alters the total binding strength of the nanotube to the nanoparticle. As the nitrogen-cobalt bond is stronger than the carbon-cobalt bond, nitrogen-cobalt bonds cause local pinning of the metal particle to the inside graphitic surface, *i.e.* nitrogen incorporation results in increased residency times and ultimately bamboo-compartment formation.

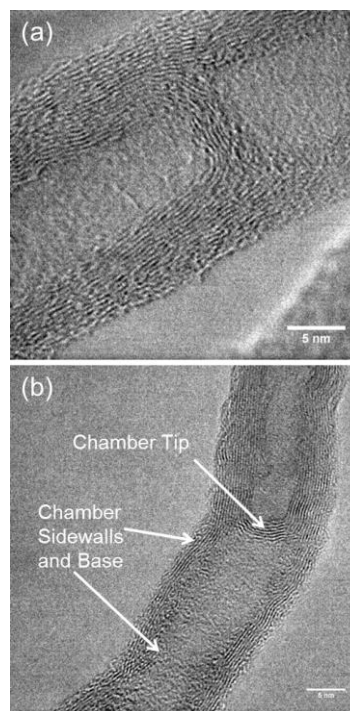


Figure 5. TEM images of N-doped bamboo-structured carbon nanotubes.

Due to the growth mechanism of the BCNTs, the tip is formed first and then the sidewalls are formed, leading to longer interaction time of the nanoparticle with the tip compared to the sidewalls. Also, as the nanoparticle elongates, the tip and the top of each chamber is supplied with more carbon and the layers are thicker than at the base of the chamber. During the initial phase of growth of the BCNTs, the thickness of the first chamber tip is

the same as the chamber thickness throughout each compartment of the tube shown in Figure 1(e). The similarity between the chamber tips and the actual BCNT tip shows that the initial formation of the tube is repeated at regular intervals controlled by the particle elongation and retraction as described above. Third stage continuous growth of more or less defect-free MWNTs does thus not occur when nitrogen is incorporated as a dopant in the CNT, as our simulations show that nitrogen itself is a local pinning agent. Instead BCNTs are formed, which only involve stage one and stage two growth repeatedly. The combined evidence from our experimental findings and theoretical simulations is that incorporation of nitrogen will always increase the risk of formation of BCNTs rather than SWNTs or MWNTs since nitrogen itself contributes to the production of bamboo-compartments. This effect could possibly be counteracted by other growth parameters, e.g. temperature or inclusions of plasma energy.

The formation of BCNTs is indicative of both surface and bulk diffusion of carbon throughout the catalyst particle during growth. If the diffusion of carbon and nitrogen through the nanoparticle is purely at the surface, the supply of carbon to the tip, which results in the increased layer formation in this area, would not take place. During growth, a non-encapsulated portion of the nanoparticle must remain to facilitate cracking of the carbon and nitrogen species, if this portion does not remain, nanoparticle poisoning occurs and growth ceases. Bulk diffusion of the carbon through the nanoparticle supplies carbon to the other end of the nanoparticle which allows for the formation of layers of graphitic carbon also at the tip of each compartment in the BCNTs. In MWNT growth there is only sidewall growth of a numbers of coaxial tubes which means that surface diffusion plays a more significant role. As is shown in figure 6, from other carbon structures that are found in a sample of unpurified N-doped BCNTs, layers of carbon form one at a time around the nanoparticle which also indicates a mechanism by which bulk diffusion of carbon throughout the nanoparticle is prevalent. Due to the "onion-like" formation of graphitic layers within each other, it is unlikely that carbon diffusion on the surface of the nanoparticle is the only way of delivering carbon to the carbon structure. As these layers are forming consecutively and at the same time as on adjacent nanoparticles, carbon atoms are being delivered throughout the catalyst particle to effectively form continuous graphitic layers.

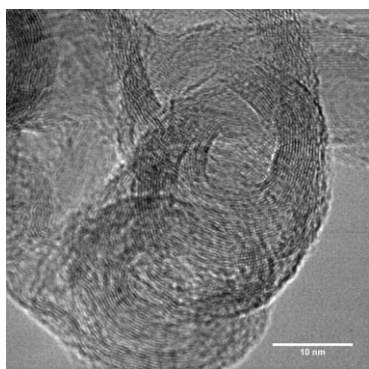


Figure 6. HRTEM of carbon product formed 4 wt. % Co/3 wt. % Mo on MgO using CH₄ and acetonitrile as the carbon and nitrogen sources showing the encapsulation effect and bulk diffusion of carbon throughout nanoparticle during growth.

The binding energy between the graphitic carbon structure and the catalytic metal nanoparticle influences both the catalytic activity and the type of nanotube which is grown. Previous reports show that combining two metals that cannot be used alone to form CNTs, one with too weak carbon-metal bonds (Cu, Pd) and one with too strong carbon-metal bonds (Mo, W) can be used to grow BCNTs^[12c, 12d]. Heterometallic nanoparticles, Cu/W, Cu/Mo, Pd/W, form favourable carbon-metal binding strengths for producing nanotubes. However, the local stronger bonds of carbon to individual Mo or W atoms on the particle surface results in BCNT growth. This difference in the binding strength of carbon to Mo or W causes variations in particle retention times and repeated elongations of the metal particle. The incorporation of nitrogen into the nanotube also leads to stronger binding between the graphitic structures and the metal nanoparticle, although not as pronounced as in the case of Mo or W doped Cu/Pd particles. However, these stronger nitrogen-metal bonds act as local points of increased binding strengths, i.e. pin-points, resulting in BCNT formation from catalysts that would have otherwise grown SWNTs or MWNTs without a nitrogen source. We propose that defective BCNTs form rather than more crystalline SWNTs or MWNTs when stronger binding defects/dopants are present either in the metal particle or in the CNT product.

Conclusion

N-doped CNTs were synthesised using traditional CVD methods. Upon the addition of a nitrogen feedstock gas to the reaction zone, BCNTs inevitably resulted. Catalysts that traditionally form SWNTs or MWNTs produced BCNTs with the addition of nitrogen to the structure. XPS analysis was used to measure the total nitrogen content of the purified tubes. Density functional theory calculations showed that the binding strength of nitrogen to cobalt is stronger than the binding strength of carbon to cobalt. This difference in the binding energies causes local points of increased binding strength to the nanoparticle within the graphitic layers formed during growth. These local points of increased binding strength increase the interaction time and strength of the graphitic layers to the nanoparticle which causes the nanoparticle to elongate during growth of the tubes. This elongation and subsequent contraction leads to the formation of the BCNTs. Overall we have synthesised N-doped BCNTs with 2.5 atom % of nitrogen within the nanotubes, with an explanation of the resulting mechanism of growth.

Experimental Section

Catalyst Preparation. The MgO support was prepared by the decomposition of Mg₂(OH)₂CO₃ at 450 °C for 6 hr in a furnace. Aqueous solutions of cobalt nitrate (Co(NO₃)₂·7H₂O) and ammonium molybdate ((NH₄)₂MoO₄·H₂O) were mixed with 2 g of MgO support, sonicated for 1 hr, dried in air and calcined at 500 °C. In all cases the dried powders were sintered at 500 °C for 6 h to produce the catalyst. The metal content of the catalyst was recorded as a weight percent with regard to the MgO support.

Chemical Vapor Deposition of Carbon. Carbon nanostructures were synthesised by metal catalyst assisted chemical vapor CVD of methane. 0.3 g of the catalyst powder was placed in a quartz tube in the middle of a furnace and heated to a reaction temperature of

850 °C in a reducing atmosphere H₂/Ar (20/180 mL min⁻¹) for 30 min. After catalyst activation, methane was introduced into the reaction chamber (flow rate of 100 mL min⁻¹) with various nitrogen sources (ammonia, pyridine or acetonitrile) for 60 min and the system was allowed to cool to room temperature. The as-obtained material was treated with 6 M HCl and rinsed with water to remove the metal and MgO catalyst support from the carbon nanotubes generated.

Characterisation. Transmission electron microscopy (TEM) was performed on JEOL 2000 FX and JEOL 2100 instruments operating at 120 kV or 200 kV. Samples for TEM analysis were prepared in ethanol and deposited onto Cu or Ni grids. Raman spectra were recorded on a Renishaw 1000 Raman system in an ambient atmosphere using a 5 mW He-Ne laser ($\lambda = 514.5$ nm) and a CCD detector. X-ray photoelectron spectroscopy (XPS) characterisation of the samples was carried out on a VSW Atomtech system using a non-monochromated Al X-ray source. CNTs were placed under vacuum to remove air from the sample. Survey spectra were taken as an average of 5 scans captured at a pass energy of 100 eV, a step size of 0.7 eV and a dwell time of 0.1 s. Core level spectra were taken as an average of 30 scans captured at a pass energy of 20 eV, a step size of 0.2 eV and a dwell time of 0.1 s.

Simulations. The ability of a Co nanoparticle to stabilise the growing end of a nitrogen-doped nanotube was investigated by calculating the binding energy of (3,3), (5,0), (5,5) and (10,0) SWNTs adhered to Co clusters of suitable diameter. Calculated binding energies were compared to binding energies previously reported for undoped CNTs²⁸. In each calculation the CNT contained one substitutional nitrogen atom representing doping of 1.7 to 3.5 atom % for (5,5), (10,0) and (3,0), (5,0) nanotubes respectively. The binding energies were calculated within density functional theory using the Vienna ab initio simulation package (VASP)^[18]. The projector augmented wave method was used^[19], along with the Perdew-Wang formulation of the generalised gradient approximation (GGA) exchange and correlation functional^[19b, 20]. A plane wave cut off of 400 eV was used for the relaxation of the nanotube systems, followed by a single-point at 500 eV. The simulation box for (3,3) and (3,3)-Co₁₃ was 10 × 10 × 20 Å, for (5,0) and (5,0)-Co₁₃ was 10 × 10 × 30 Å and was 15 × 15 × 30 Å for (5,5), (5,5)-Co₅₅, (10,0) and (10,0)-Co₅₅. For the smaller systems a Gaussian smearing of 0.05 eV was used, while the Methfessel-Paxton scheme 36 was used for the Co₅₅ systems. Spin-polarised calculations were performed in all cases and the nanotube structures were relaxed without symmetry constraints.

Acknowledgements

((The authors acknowledge financial support from Science Foundation Ireland (Grant 08/CE/11432), the Tyndall National Access Programme (NAP Project 160), and the Irish Research Council for Science, Engineering and Technology (IRCSET). Computational resources were provided by SFI/HEA Irish Centre for High-End Computing (ICHEC), SFI/HEA through local computing cluster at Tyndall. This research was also enabled by the Higher Education Authority Program for Research in Third Level Institutions (2007-2011) via the INSPIRE programme.

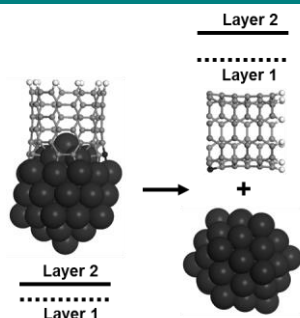
Keywords: Nanotubes · Doping · Nitrogen · Catalyst · DFT

- [1] a) T. W. Odom, J.-L. Huang, P. Kim, C. M. Lieber, *Nature* **1998**, 391, 62-64; b) T. W. Odom, J.-L. Huang, P. Kim, C. M. Lieber, *J. Phys. Chem. B* **2000**, 104, 2794-2809; c) <http://standards.ieee.org/announcements/PRNESR.html> **2007**.
- [2] a) K. Gong, F. Du, Z. Xia, M. Dustock, L. Dai, *Science* **2009**, 323, 760-764; b) S. H. Lim, H. I. Elim, X. Y. Gao, A. T. S. Wee, W. Ji, J. Y. Lee, J. Lin, *Phys. Rev. B* **2006**, 73, 045402; c) I. O. Maciel, J. Campos-Delgado, E. Cruz-Silva, M. A. Pimenta, B. G. Sumpter, V. Meunier, F. López-Urías, E. Muñoz-Sandoval, H. Terrones, M. Terrones, A. Jorio, *Nano Lett* **2009**, 9, 2267-2272.
- [3] Y. Huang, J. Gao, R. Lie, *Synthetic Metals* **2000**, 113, 251-255.
- [4] a) L. G. Bulusheva, A. V. Okokrub, A. G. Kudashov, I. P. Asanov, O. G. Abrosimov, *Eur. Phys. J. D* **2005**, 34, 271-274; b) M. Terrones, A. S. Souza Filho, A. M. Rao, *Topics in Applied Physics* **2008**, 111/2008, 531-566.
- [5] M. Terrones, *Annu. Rev. Mater. Res.* **2003**, 33, 419-501.
- [6] M. Glerup, M. Castignolles, M. Holzinger, G. Hug, A. Loiseau, P. Bernier, *Chem. Commun.* **2003**, 2542-2543.
- [7] a) J. W. Jang, C. E. Lee, S. C. Lyu, T. J. Lee, C. J. Lee, *Appl. Phys. Lett.* **2004**, 84, 2877-2879; b) J. Liu, S. Webster, D. L. Carroll, *J. Phys. Chem. C* **2005**, 109, 15769-15774; c) J. Liu, S. Webster, D. L. Carroll, *Appl. Phys. Lett.* **2006**, 88, 213119; d) M. Terrones, P. M. Ajayan, F. Banhart, X. Blase, D. L. Carroll, J.-C. Charlier, R. Czerw, B. Foley, N. Grobert, R. Kamalakaran, P. Kohler-Redlich, M. Ruhle, T. Seeger, H. Terrones, *Appl Phys A* **2002**, 74, 355-361.
- [8] a) E. Cruz-Silva, D. A. Cullen, L. Gu, J. Manuel Romo-Herrera, E. Muñoz-Sandoval, F. López-Urías, B. G. Sumpter, V. Meunier, J.-C. Charlier, J.-C. Smith, D. J. Smith, H. Terrones, M. Terrones, *ACS Nano* **2008**, 2, 441-448; b) W. K. Hsu, S. Firth, P. Redlich, M. Terrones, H. Terrones, Y. Q. Zhu, N. Grobert, A. Schilder, R. J. H. Clark, H. W. Kroto, D. R. M. Walton, *J. Mater. Chem.* **2000**, 10, 1425-1429.
- [9] A.-C. Dupuis, *Progress in Materials Science* **2005**, 50, 929-961.
- [10] a) F. Ding, A. Rosén, E. E. B. Campbell, L. K. L. Falk, K. Bolton, *J. Phys. Chem. B* **2006**, 110, 7666-7670; b) M. Stadermann, S. P. Sherlock, J.-B. In, F. Fornasiero, H. G. Park, A. B. Artyukhin, Y. Wang, J. J. De Yoreo, C. P. Grigoropoulos, O. Bakajin, A. A. Chernov, A. Noy, *Nano Lett* **2009**, 9, 738-744.
- [11] X. X. Zhang, Z. Q. Li, G. H. Wen, K. K. Fung, J. Chen, Y. Li, *Chem. Phys. Lett.* **2001**, 333, 509.
- [12] a) F. Ding, P. Larsson, J. A. Larsson, R. Ahuja, H. Duan, A. Rosen, K. Bolton, *Nano Letters* **2007**, Web 12/28/2007, 5.1; b) P. Larsson, J. A. Larsson, R. Ahuja, F. Ding, B. I. Yakobson, H. Duan, A. Rosén, K. Bolton, *Phys. Rev. B* **2007**, 75, 115419; c) Z. Li, J. A. Larsson, P. Larsson, R. Ahuja, J. M. Tobin, J. O'Byrne, M. A. Morris, G. Attard, J. D. Holmes, *J. Phys. Chem. C* **2008**, 112, 12201; d) J. P. O'Byrne, Z. Li, J. M. Tobin, J. A. Larsson, P. Larsson, R. Ahuja, J. D. Holmes, *J. Phys. Chem. C* **2010**, 114, 8115-8119.
- [13] S. Helveg, C. López-Cartes, J. Sehested, P. L. Hansen, B. S. Clausen, J. R. Rostrup, F. Abild-Pederson, J. K. Nørskov, *Nature* **2004**, 427, 426-429.
- [14] M. S. Dresselhaus, G. Dresselhaus, R. Saito, A. Jorio, *Physics Reports* **2004**.
- [15] a) C. J. Lee, J. H. Park, J. Park, *Chem. Phys. Lett.* **2000**, 323, 560-565; b) J. Liu, M. Shao, X. Chen, W. Yu, X. Liu, Y. Qian, *J. Am. Chem. Soc.* **2003**, 125, 8088-8089.
- [16] a) D. Cremer, A. Wu, A. Larsson, E. Kraka, *J. Mol. Model.* **2000**, 6, 396-412; b) J. A. Larsson, D. Cremer, *J. Mol. Struct.* **1999**, 485-486, 385-407.
- [17] M. Lin, J. P. Y. Tan, C. Boothroyd, K. P. Loh, E. Tok, S.; Y. L. Foo, *Nano Lett* **2007**, 7, 2234.
- [18] a) G. Kresse, J. Furthmüller, *Phys. Rev. B* **1996**, 54, 11169-11186; b) G. Kresse, J. Hafner, *Phys. Rev. B* **1993**, 47, 558-561; c) G. Kresse, J. Hafner, *Phys. Rev. B* **1994**, 49, 14251; d) G. Kresse, D. Joubert, *Phys. Rev. B* **1999**, 59.
- [19] a) P. E. Blöchl, *Phys. Rev. B* **1994**, 50, 17953-17979; b) J. P. Perdew, J. A. Chevary, S. H. Vosko, K. A. Jackson, M. R. Pederson, D. J. Singh, C. Fiolhais, *Phys. Rev. B* **1992**, 46, 6671-6687.
- [20] J. P. Perdew, J. A. Chevary, S. H. Vosko, K. A. Jackson, M. R. Pederson, D. J. Singh, C. Fiolhais, *Phys. Rev. B* **1993**, 48, 4978.

Received: ((will be filled in by the editorial staff))

Published online: ((will be filled in by the editorial staff))

Nitrogen-doped bamboo-structured carbon nanotubes have been successfully grown using a series of cobalt/molybdenum catalysts. The growth of bamboo-structured nanotubes in the presence of nitrogen, in preference to single-walled and multi-walled nanotubes, is due to the greater binding energy of nitrogen for cobalt in the catalyst compared to the binding strength of carbon to cobalt, as determined by density functional theory.



*Justin P. O'Byrne, Zhonglai Li, Sarah L. Jones, Peter G. Fleming, J. Andreas Larsson, Michael A. Morris and Justin D. Holmes**

Page No. – Page No.

Nitrogen-Doped Carbon Nanotubes: Growth, Mechanism and Structure